

L- and Θ -curve approaches for the selection of regularization parameter in geophysical diffraction tomography

E.T.F. Santos^a, A. Bassrei^{b,*}

^aCEFET/BA and Institute of Geosciences Federal University of Bahia, Salvador, Brazil

^bInstitute of Physics & Research Center in Geophysics and Geology Federal University of Bahia, Caixa Postal 1001, 40001-970 Salvador BA, Brazil

Received 2 May 2006; received in revised form 10 August 2006; accepted 27 August 2006

Abstract

Since inverse problems are usually ill-posed it is necessary to use some method to reduce their deficiencies. The method that we choose is the regularization by derivative matrices. When a first derivative matrix is used the order is called the first. Then, second-order regularization is when the matrix is formed by second-order differences, and order zero means that the regularization matrix is the identity. There is a crucial problem in regularization, which is the selection of the regularization parameter λ . We used the L-curve as a tool for the selection of λ , and we propose a new extension, which we call the Θ -curve. The tool was applied in geophysical diffraction tomography in two acquisition geometries: cross-hole and vertical seismic profile (VSP), where the goal is to obtain the 2-D velocity distribution from the measured values of the scattered acoustic field. We present several simulation results with synthetic data, for the three regularization orders mentioned above. We validate the necessity of some kind of regularization, as well as the feasibility of both parameter selection approaches.

© 2006 Elsevier Ltd. All rights reserved.

Keywords: Inverse problems; Diffraction tomography; Regularization; Regularization parameter; L-curve; Θ -curve

1. Introduction

The main purpose of exploration geophysics for hydrocarbons is to provide trustworthy images of the subsurface, which can indicate potential hydrocarbon reservoirs. Exploration seismology, better known as seismics, is the area of applied geophysics most employed for the subsurface imaging in hydrocarbons reservoirs. And within seismics,

tomography is incorporated as a suitable method of data inversion. In this work, we use geophysical diffraction tomography where the input data is the scattered acoustic field measured at the receivers, and the velocity of the 2-D medium is the inversion output. Instead of using the classical approach of diffraction tomography in geophysics, i.e., the Fourier projection theorem (Devaney, 1984; Slaney et al., 1984; Wu and Toksöz, 1987), we use a matrix formulation approach (Thompson et al., 1994; Reiter and Rodi, 1996; Rocha Filho et al., 1996, 1997). The main advantages of the matrix formulation are: (1) the option of having irregular spacing (i) between sources, (ii) between receivers

*Corresponding author. Tel.: +55 71 3203 8508; fax: +55 71 3203 8501.

E-mail addresses: etfs@cpgg.ufba.br (E.T.F. Santos), bassrei@cpgg.ufba.br (A. Bassrei).

and (iii) between sources and receivers (all very common in practical situations with real data); and (2) the possibility to study, in a better way, the ill-posedness of the inverse problem. The main disadvantage is the cost in terms of computation time. For forward modeling, we compute the scattered acoustic field from a given 2-D velocity distribution. The field is obtained by a second-order finite difference scheme and the tomographic matrix by a first-order Born approximation. One common way to calculate the inverse matrix is by the generalized inverse through singular value decomposition (SVD).

Since geophysical diffraction tomography is an ill-posed inverse problem, it is necessary to use some tool to reduce this deficiency. The tool that we choose is the regularization of the inverse problem by derivative matrices, known in the literature by several names, (e.g. the Tikhonov regularization). This tool has an important input parameter called the regularization parameter λ .

In the last 10 years researchers have studied the problem of finding the optimum value of λ in geophysical applications. One of first works was done by Ray and Sanchez (1994), who used regularization and the L-curve to raw tidal estimates based on Geosat altimeter data. The estimation is based on fitting specific functions called Proudman functions as a spatial basis, which is formulated as a linear system. The fitting coefficients are obtained solving the corresponding least-squares problem using zero-order regularization. Then, L-curve is applied to obtain the optimal regularization parameter. Yao and Roberts (1999), presented an algorithm for the practical choice of the regularization parameter in linear seismic tomographic inversion. Two criteria for the choice of the regularization parameter were investigated. The first approach assumes that the norm of the errors in observed data is known accurately and searches the regularization parameter associated with this error using Newton's method. The second approach is the application of the generalized cross-validation (GCV), which chooses the regularization parameter associated with the best average prediction for all possible omissions of one datum, corresponding to the minimum of the GCV function. More recently, Farquharson and Oldenburg (2004) compared two automatic ways of estimating the best regularization parameter to non-linear inverse problems: the GCV and L-curve. These criteria initially proposed for linear problems are applied to each iteration

of linearized inverse problems, in a typical iterative process to obtain the linearized solution to the corresponding non-linear problem. Thus, the best λ is estimated for each linearized iteration. To ensure that the regularization parameter decreases along iterations, an attenuation factor is multiplied by the regularization parameter at the last iteration to limit the next maximum allowable parameter.

Some other relevant works that consider the aspect of parameter selection, either generally, or in geophysical applications are Hansen (1992, 1998), Bouman and Sauer (1993), Hansen and O'Leary (1993), Hanke (1996), Hanke and Raus (1996), Reginska (1996), Vogel (1996), Belge et al. (2002), Calvetti et al. (1999), Kilmer and O'Leary (2001), Soupios et al. (2001, 2003), Castellanos et al. (2002) and McCarthy (2003).

In the present work, to our knowledge the first one in geophysical diffraction tomography using regularization with search for the optimum parameter, we employ the L-curve and an extension of it, which we call the Θ -curve, in cross-hole and vertical seismic profile (VSP) geophysical diffraction tomography. In the L-curve the x -axis represents the error between the observed data and the calculated one, and the y -axis represents the amount of regularization of the solution. The L-curve was reintroduced in the literature of inverse problems by Hansen (1992, 1998) and he also produced a toolbox (Hansen, 1992). Hansen's book (1998) is a very good source of information for a more rigorous treatment of the L-curve.

2. Regularization, L- and Θ -curve

Consider a modeling process where the input of a system is described by certain parameters contained in \mathbf{m} and the output is described as $A\mathbf{m} (= \mathbf{d})$ which is a linear transformation on \mathbf{m} . If the vector \mathbf{d} describes the observed output of the system, the problem is to "choose" the parameters \mathbf{m} in order to minimize in some sense, the difference between the observed \mathbf{d} and the prescribed output of the system $A\mathbf{m}$. If we measure this difference through the norm $\|\cdot\|$, our task is to find the value of \mathbf{m} that minimizes $\|A\mathbf{m} - \mathbf{d}\|_2$, where the $M \times N$ matrix A and the data vector \mathbf{d} with M elements are provided. This is called a least-squares problem, which can be formally stated as follows. Considering the basic relationship $\mathbf{d} = A\mathbf{m}$, we wish to minimize the error

using the following objective function:

$$\Phi(\mathbf{m}) = (\mathbf{d} - A\mathbf{m})^T \cdot (\mathbf{d} - A\mathbf{m}). \tag{1}$$

The estimated solution, also called least-squares solution, is

$$\mathbf{m}^{est} = (A^T A)^{-1} A^T \mathbf{d}. \tag{2}$$

Least-squares solutions very often do not provide good results and sometimes they do not even exist. In order to solve this problem we use a tool of regularization or smoothing: the ill-conditioning of the matrix A is regularized and the unstable least-squares estimate \mathbf{m}^{est} is consequently smoothed to greatly reduce the possibility of wild noise-induced fluctuation in \mathbf{d} , hopefully without distorting the resulting smoothed image too far from the true \mathbf{m} (Titterton, 1985).

The concept of regularization was introduced by Tikhonov in 1963 in order to improve the quality of the inversion. This theory was studied by many researchers, and we use the Twomey (1963) approach. See Bassrei and Rodi (1993) about the names and history in regularization theory. Consider the following objective function:

$$\Phi(\mathbf{m}) = \lambda(D_l \mathbf{m})^T D_l \mathbf{m} + \mathbf{e}^T \mathbf{e}, \tag{3}$$

where λ is the regularization parameter and D_l is the l -th-order derivative matrix. If $\partial\Phi(\mathbf{m})/\partial\mathbf{m} = 0$, then the estimated model is given by

$$\mathbf{m}^{est} = (A^T A + \lambda D_l^T D_l)^{-1} A^T \mathbf{d}. \tag{4}$$

Notice that if $\lambda = 0$ we obtain the standard least squares, and the least squares is said to be damped if $D_0^T D_0 = I$. If D is the first derivative matrix then the regularization is called to be first order and so on. Each 2D model is scanned line by line to be represented by a single vector, i.e., rasterized. It simplifies the form of the discrete derivative approximation matrix, which resembles a regular pattern. Thus, the matrices D_1 and D_2 may be schematized by the following templates:

$$D_1 = \begin{pmatrix} -1 & 1 & 0 & 0 & 0 & 0 & 0 & \dots & 0 \\ 0 & -1 & 1 & 0 & 0 & 0 & 0 & \dots & 0 \\ \vdots & & & \vdots & \ddots & \vdots & & & \dots \\ 0 & \dots & 0 & 0 & 0 & 0 & -1 & 1 & 0 \\ 0 & \dots & 0 & 0 & 0 & 0 & 0 & -1 & 1 \end{pmatrix} \tag{5}$$

and

$$D_2 = \begin{pmatrix} 1 & -2 & 1 & 0 & 0 & 0 & 0 & \dots & 0 \\ 0 & 1 & -2 & 1 & 0 & 0 & 0 & \dots & 0 \\ \vdots & & & \ddots & & & & & \dots \\ 0 & \dots & 0 & 0 & 0 & 1 & -2 & 1 & 0 \\ 0 & \dots & 0 & 0 & 0 & 0 & 1 & -2 & 1 \end{pmatrix}. \tag{6}$$

The L-curve knee (Fig. 1) represents a trade-off between smoother solutions with higher errors and rougher solutions with smaller errors. Thus, the knee detection at the L-curve is an heuristic criterion to select the most appropriate solution. Solutions near to the curve knee are also acceptable. Thus, one can achieve a solution that simultaneously satisfies the criteria of error minimization, smoothness and also with physical meaning.

The detection of the L-curve corner was performed using Hansen’s toolbox. A number of different definitions have been proposed for the best estimation of the L-curve corner (Calvetti et al., 2002; Belge et al., 2002; Kilmer and O’Leary, 2001; Hansen, 1992, 1998).

Considering this curve approximately L-shaped, one can find its knee searching the maximum curvature point (Hansen, 1992; Hansen and O’Leary, 1993). Although, secondary inflexions may occur, which may result in the wrong detection of the best regularization parameter. Thus, the automatic method of knee detection adopted in this toolbox may lead sometimes to inadequate regularization parameters. Due to this problem, sometimes

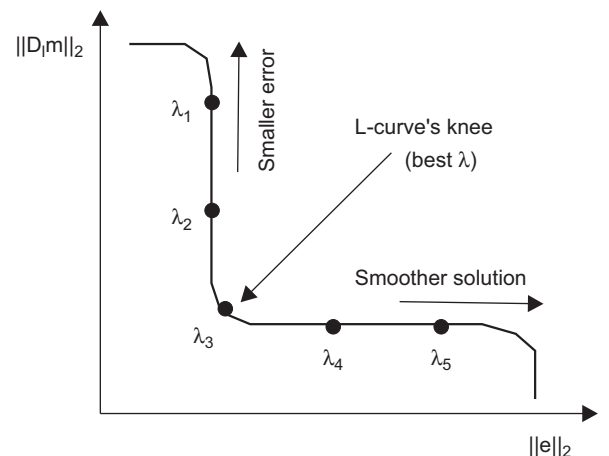


Fig. 1. Schematic representation of L-curve.

it is necessary to select the best regularization parameter by visual inspection of the L-curve and a manual detection of its knee. Belge et al. (2002) adopted the point closest to the origin of L-curve graph as an estimation of the L-curve corner. It works fine when the curve is clearly L-shaped, but it may fail when the inflexion at knee significantly differs from a straight angle because other points outside knee may be closer to the origin.

Thus, a criterion that identifies the L-curve corner should be flexible enough to tolerate certain deviations from its ideal L-shape and still correctly identifies correctly its corner. We adopted a different criterion based on a curve representing the cosine of angles between adjacent segments of L-curve discrete representation, which we named Θ -curve. Where the curve is locally straight, the angle tends to zero, leading the cosine of this angle to one. Near the L-curve knee, the angle tends to be greater than its neighbors, leading the cosine to values less than one. Thus, smaller cosine values are associated with inflexions of the curve, which lead us to inspect the minima of the Θ -curve to find the knee of the L-curve and consequently the best regularization parameter (Fig. 2). The method developed to select the best regularization parameter is based on the detection of the first local minimum of the Θ -curve. This minimum is automatically detected where the first derivative is close to zero and the second derivative is positive, adopting thresholds due to the discretization and arithmetic computer precision. Thus, the first occurrence of minimum at Θ -curve is

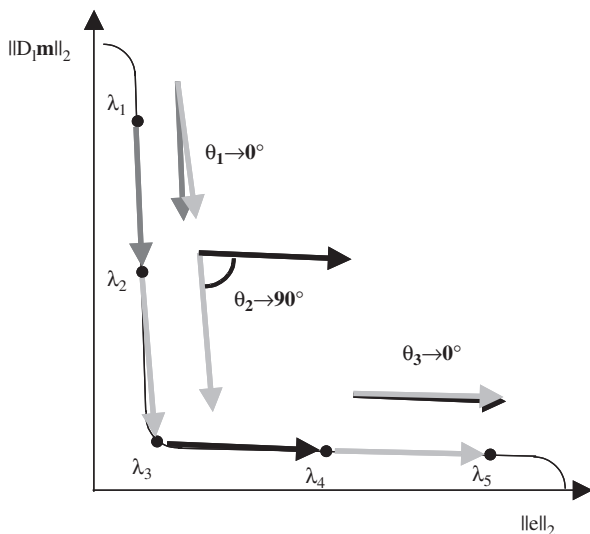


Fig. 2. Schematic representation for the construction of Θ -curve.

associated with the knee of L-curve, giving us the best regularization parameter. Further inflexions of the L-curve were discarded because only the first local minimum of Θ -curve is associated with L-curve knee. This avoids the wrong regularization parameter detection described before, when one adopts the criterion of maximum curvature of the L-curve.

3. Diffraction tomography modeling via Born approximation

The wave equation is given by

$$\nabla^2 U(\mathbf{r}, t) = \frac{1}{c^2(\mathbf{r})} \frac{\partial^2 U(\mathbf{r}, t)}{\partial t^2}, \quad (7)$$

where $U(\mathbf{r}, t)$ is the solution, either displacement or pressure, and $c(\mathbf{r})$ is the acoustic velocity of the medium. Considering that the solution can be written as $U(\mathbf{r}, \omega, t) = e^{-i\omega t} P(\mathbf{r}, \omega)$, which represents a harmonic dependence with time, we obtain the Helmholtz equation:

$$[\nabla^2 + k^2]P(\mathbf{r}, \omega) = 0, \quad (8)$$

where the two-dimensional (2-D) wavenumber is given by $k = k(\mathbf{r}, \omega) = \sqrt{k_x^2 + k_y^2}$. The conditions for the imaging are that the medium is acoustic and 2-D, and the propagation of the incident field is within a limited area $A(\mathbf{r}')$, the background, with constant velocity c_0 . The object function is defined as

$$O(\mathbf{r}) = 1 - \frac{c_0^2}{c^2(\mathbf{r})} \quad (9)$$

and represents the perturbation of the velocity in each point in relation to c_0 . Redefining the wavenumber as function of $O(\mathbf{r})$, and substituting it in the Helmholtz equation, we obtain

$$[\nabla^2 + k^2]P_S = k_0^2 O(\mathbf{r})[P_O + P_S], \quad (10)$$

where P_O is the incident field and P_S is the scattered field. The last differential equation has the following integral solution, known as Lippmann–Schwinger equation (Lo and Inderwiesen, 1994):

$$P_S(\mathbf{r}) = -k_0^2 \int_{A(\mathbf{r}')} O(\mathbf{r}') G(\mathbf{r}|\mathbf{r}') [P_O(\mathbf{r}') + P_S(\mathbf{r}')] d\mathbf{r}'. \quad (11)$$

In the inverse scattering procedure, we consider the knowledge of the scattered field, so that the object function is the unknown function, and the

Table 1
 λ_{best} and ε_{rms}^c (%) of all simulations

Model	Method	λ_{best}	ε_{rms}^c (%)
Example 1—diffractor point cross-hole	Order 0: L-curve	0.0008	0.0742
	Order 0: Θ -curve	0.0666	0.0572
	Order 1: L-curve	0.0006	0.0687
	Order 1: Θ -curve	0.0769	0.0520
	Order 2: L-curve	0.0003	0.0703
	Order 2: Θ -curve	0.0514	0.0505
	Least squares	—	0.0568
Example 2—plus pod cross-hole	Order 0: L-curve	0.0060	0.6895
	Order 0: Θ -curve	0.0045	0.7750
	Order 1: L-curve	0.0111	0.5175
	Order 1: Θ -curve	0.0061	0.5506
	Order 2: L-curve	0.0041	0.5331
	Order 2: Θ -curve	0.0038	0.5385
	Least squares	—	2.6842
Example 3—reef cross-hole	Order 0: L-curve	0.1234	0.5130
	Order 0: Θ -curve	0.1322	0.5107
	Order 1: L-curve	0.1599	0.5125
	Order 1: Θ -curve	0.3035	0.4823
	Order 2: L-curve	0.2449	0.5309
	Order 2: Θ -curve	0.4784	0.4856
	Least squares	—	0.5260
Example 4—reef VSP	Order 0: L-curve	0.2139	0.5953
	Order 0: Θ -curve	0.2256	0.5938
	Order 1: L-curve	0.2783	0.5494
	Order 1: Θ -curve	0.2971	0.5456
	Order 2: L-curve	0.8463	0.5278
	Order 2: Θ -curve	0.5867	0.5423
	Least squares	—	0.6076

integral solution becomes an integral equation. The above equation is non-linear and the linearization is achieved, for example, via the first-order Born approximation, which is only valid for the weak scattering of the incident field. The total field is $P_T(\mathbf{r}) = P_O(\mathbf{r}) + P_S(\mathbf{r})$ and $P_S(\mathbf{r}) \ll P_O(\mathbf{r})$, so that we have $P_T(\mathbf{r}) = P_O(\mathbf{r})$. Thus we obtain a linear relation between $O(\mathbf{r})$ and $P_S(\mathbf{r})$:

$$P_S(\mathbf{r}) = -k_0^2 \int_{A(\mathbf{r})} O(\mathbf{r}') G(\mathbf{r}|\mathbf{r}') P_O(\mathbf{r}') d\mathbf{r}'. \quad (12)$$

We represent the incident field by a source in \mathbf{r}_S through the Green's function:

$$P_O(\mathbf{r}') = G(\mathbf{r}'|\mathbf{r}_S) \quad (13)$$

and the scattered field in $A(\mathbf{r})$ is registered by a receptor in \mathbf{r}_G :

$$P_S(\mathbf{r}_S, \mathbf{r}_G) = -k_0^2 \int_{A(\mathbf{r}')} O(\mathbf{r}') G(\mathbf{r}'|\mathbf{r}_S) G(\mathbf{r}_G|\mathbf{r}') d\mathbf{r}'. \quad (14)$$

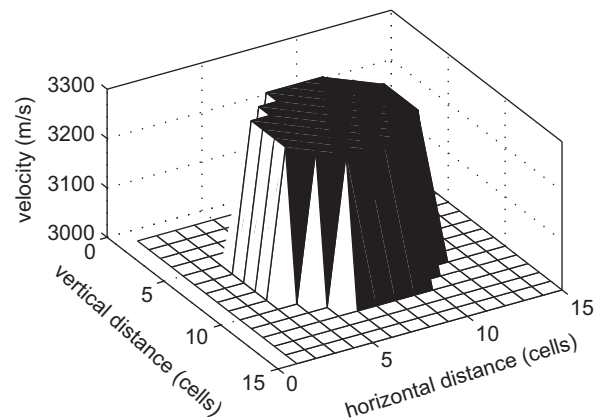


Fig. 3. Example 2—plus pod model. 3-D representation of the true model.

The discretization of the above relation leads to the linear relation $\mathbf{d} = \mathbf{A}\mathbf{m}$, which has to be inverted in order to recover $O(\mathbf{r})$. In this work the inversion is

done using SVD with regularization, which we described earlier.

4. Numerical simulation

We explore these two approaches for the selection of the regularization parameter in four synthetic examples, all with 225 blocks (15×15), i.e., the vector of model parameters has 225 components. In all numerical experiments there are 16 sources and

16 receivers, in such a way that the data set has 256 complex numbers. Since we separate the complex numbers into real and imaginary parts, we have in fact 512 numbers, making the tomographic matrix overdetermined ($512 \text{ equations} \times 225 \text{ unknowns}$). The frequency of the monochromatic wave is 200 Hz, and all the simulations were performed with noisy data. Basically we added Gaussian noise was added such that the RMS error between the original scattered field and the corrupted one is

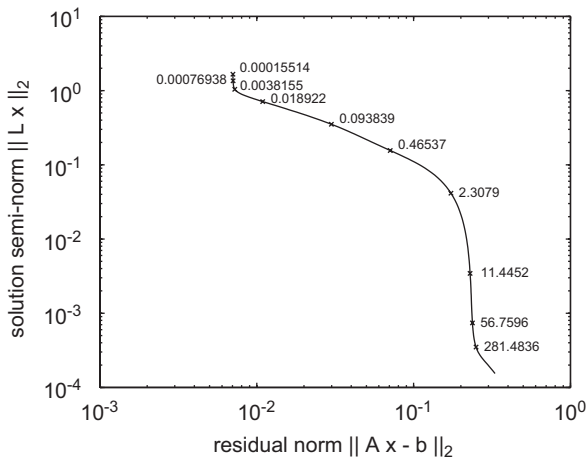


Fig. 4. Example 2—plus pod model. L-curve for second order.

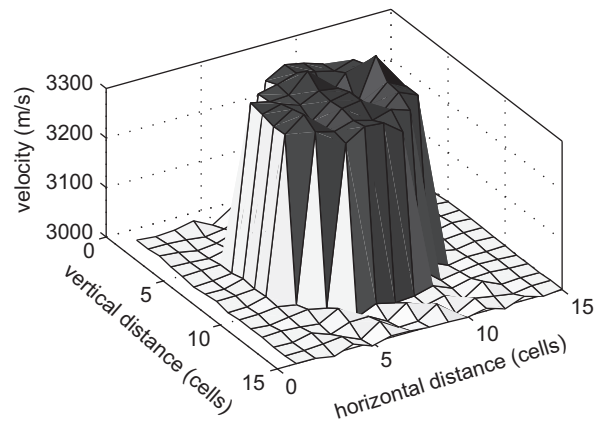


Fig. 5. Example 2—plus pod model. Reconstruction with best regularization parameter obtained from Fig. 4.

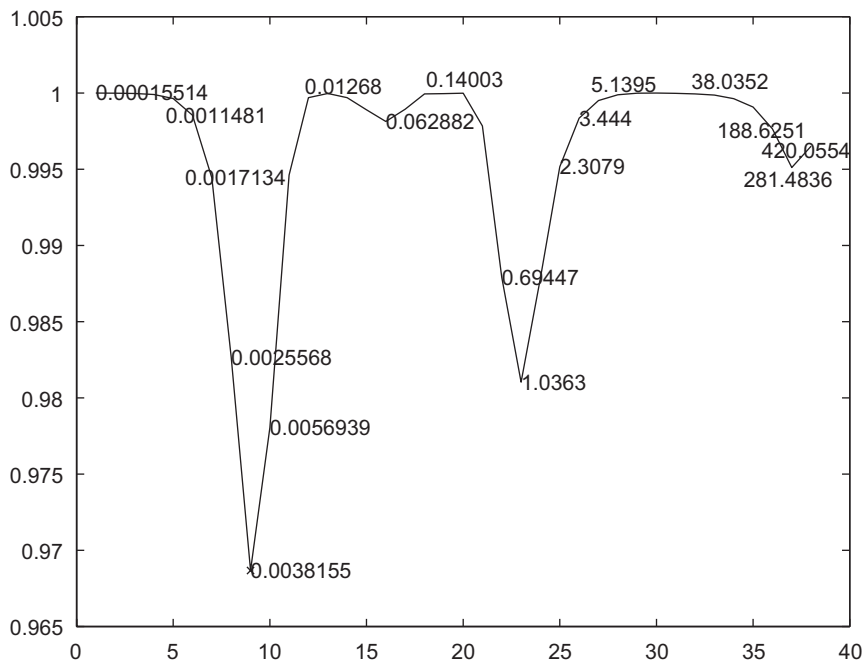


Fig. 6. Example 2—plus pod model. Θ -curve for second order.

around 1%. For each example and for each order, we produced three L-curves and three Θ -curves. Due to space limitations we show only some of the results although all simulations are summarized in Table 1, where the estimator ε_{rms}^c express the rms error of the acoustic velocity:

$$\varepsilon_{rms}^c = \frac{\sqrt{\sum_{i=1}^N (c_i^{true} - c_i^{est})^2}}{\sqrt{\sum_{i=1}^N (c_i^{true})^2}} \times 100\%. \quad (15)$$

The scattered field was computed using a second order in time and fourth order in space, finite differences scheme. We adopted a Ricker's wavelet centered around 200 Hz as the source, propagating through the medium limited by absorbing boundaries. The calculation of the scattered field can be separated into two steps: first we compute the primary field assuming a homogeneous medium with background velocity. Then we use the velocity model to compute the total field. We obtain the scattered field subtracting the primary field from the total field. The resulting scattered field was deconvolved at 200 Hz as center frequency in order to perform a monochromatic inversion. The calculated field at the source position has some differences of amplitude and phase in relation to the original Ricker's wavelet due to the modeling, which were adjusted using an average complex correction factor.

The first synthetic example simulates the diffractor point. The background medium has 4000 m/s, and the inhomogeneity (diffractor point) is represented by a single block with 4100 m/s, which means a 2.5% positive anomaly. The diffractor point is in

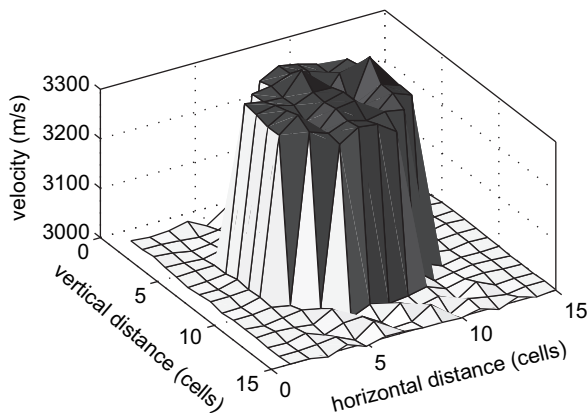


Fig. 7. Example 2—plus pod model. Reconstruction with best regularization parameter obtained from Fig. 6.

fact a 10 m \times 10 m square or half-wavelength \times half-wavelength. Due to space limitations no figures are presented for this example, but from Table 1 one can conclude that for the first and second orders the regularized solution using the Θ -curve was better than least squares. In all three orders the solutions obtained from the Θ -curve had smaller ε_{rms}^c than the ones obtained from L-curve. This discrepancy between the regularization parameters obtained from the two approaches was more accentuated in this example. In the other three sets of simulations the obtained parameters from the two approaches were close, sometimes the same.

In the second example there is a homogeneous inclusion in the form of a plus pod within the homogeneous background, which has 3000 m/s. The inclusion (plus pod) has 3300 m/s, which represents

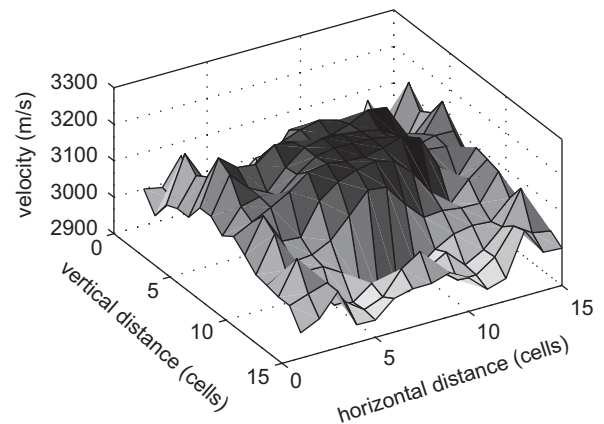


Fig. 8. Example 2—plus pod model. Least squares reconstruction.

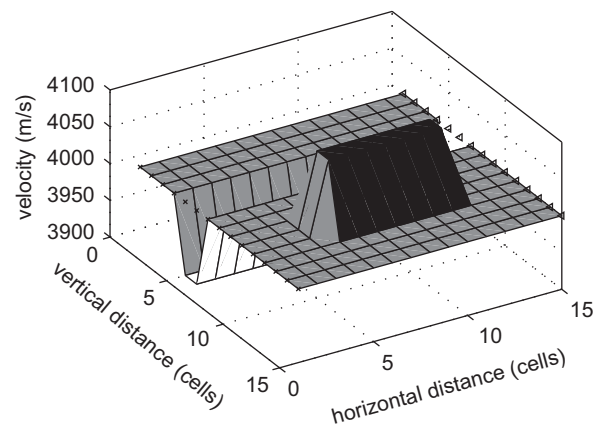


Fig. 9. Example 3—simple reef model. Cross-hole and VSP geometries data acquisition. 3-D representation of the true model.

a positive anomaly of 10%. The plus pod true model can be seen as a 3-D diagram in Fig. 3. In terms of wavelength, the plus pod has a diameter of 5.3 wavelengths. Fig. 4 shows the L-curve for the second order and Fig. 5 shows the reconstruction. Hansen’s package provided the best parameter as 0.0041. Here the L-curve obtained is more or less like the letter L shape. The Θ -curve for second order can be seen in Fig. 6 and the reconstruction in Fig. 7. Notice that the visualization of the first,

and in this case the global minimum, is straightforward, different from the corner visualization in the L-curve. The least-squares solution is presented in Fig. 8. Comparing Figs. 5 and 8, or Figs. 7 and 8, we can conclude the necessity of some kind of regularization. Comparing Figs. 5 and 7 we can conclude that the two approaches gave similar results, which is confirmed when we compare the regularization parameters and the ϵ_{rms}^c estimator.

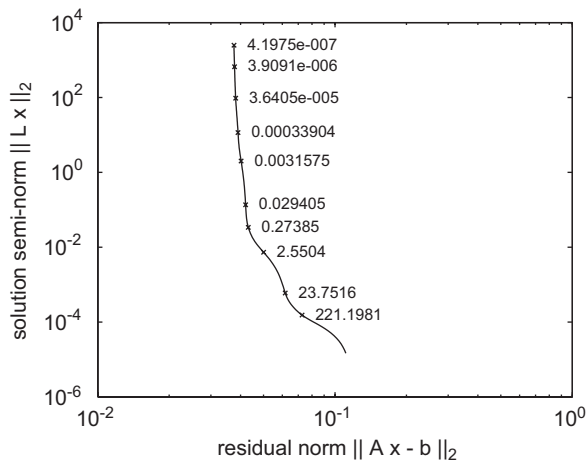


Fig. 10. Example 3—simple reef model. Cross-hole geometry data acquisition. L-curve for second order.

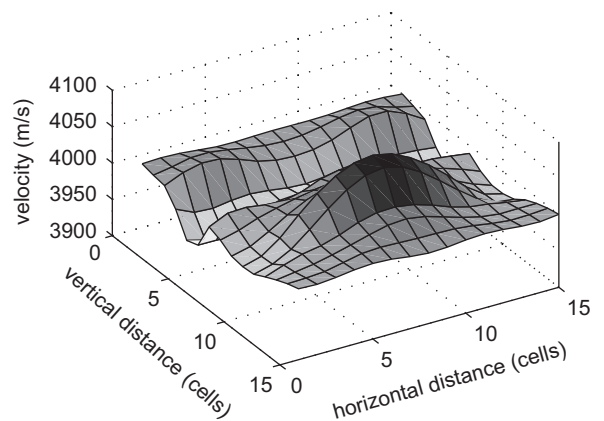


Fig. 11. Example 3—simple reef model. Cross-hole geometry data acquisition. Reconstruction with best regularization parameter obtained from Fig. 10.

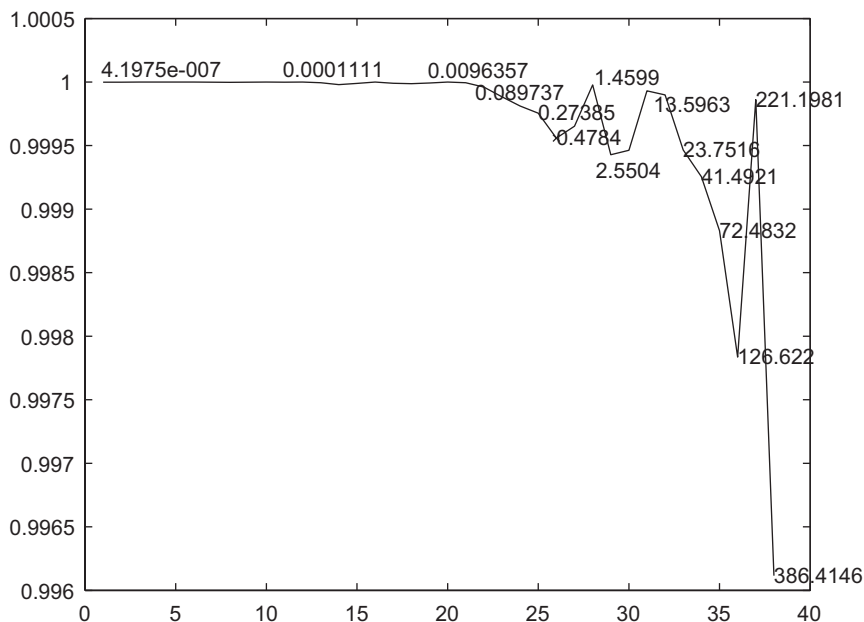


Fig. 12. Example 3—simple reef model. Cross-hole geometry data acquisition. Θ -curve for second order.

The third example, displayed in Fig. 9, is a simple representation of a reef, as a possible oil reservoir. The acquisition geometry is still the cross-hole, like the first and the second examples. There is also a low velocity layer. The background medium has 4000 m/s. The low velocity layer has 3900 m/s, which means a minus 2.5% contrast. The central inhomogeneity (the reef) has 4100 m/s which is equivalent to a plus 2.5% anomaly. In terms of wavelength the reef is 3.5 wavelengths \times 1 wavelength, and the low velocity layer is 7.5 wavelengths \times 1 wavelength. Fig. 10 shows the L-curve for second order and Fig. 11 shows the reconstruction. This is a practical example where the L-curve does not have a typical letter L shape, in such a way that it is difficult to see

the location of the L-curve corner. Hansen’s package provided the best parameter as 0.2449. For the same order the Θ -curve can be seen in Fig. 12, where we can see that the first minimum is 0.4784. As mentioned earlier we always consider only the first minimum. With this value we obtained the reconstructed tomogram showed in Fig. 13. The two results, i.e., Figs. 11 and 13 are very similar despite some difference in the ϵ_{rms}^c estimator. The least-squares solution is presented in Fig. 14. This last result is not as bad as in the previous example, but again we see that regularization is necessary.

For the VSP geometry, the true model is the same as shown in Fig. 9. The sources are still located in a hole but the receivers are now located at the surface.

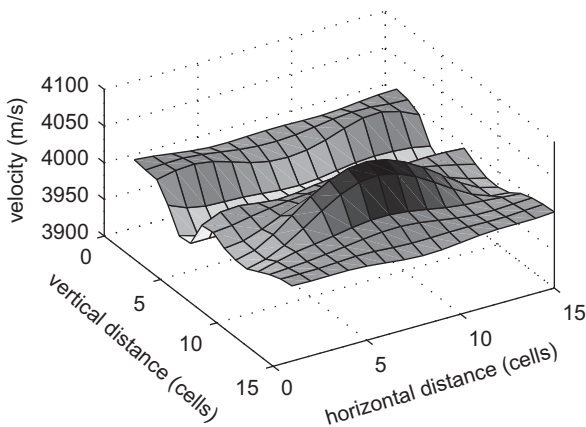


Fig. 13. Example 3—simple reef model. Cross-hole geometry data acquisition. Reconstruction with best regularization parameter obtained from Fig. 12.

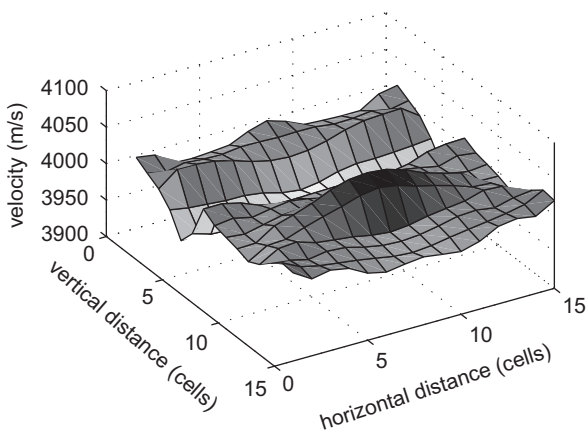


Fig. 14. Example 3—simple reef model. Cross-hole geometry data acquisition. Least-squares reconstruction.

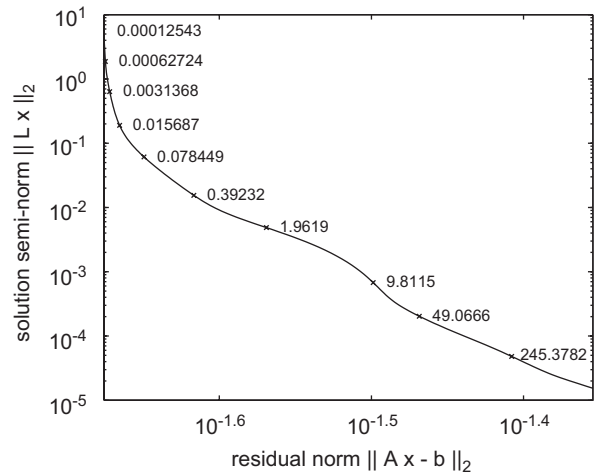


Fig. 15. Example 4—simple reef model. VSP geometry data acquisition. L-curve for second order.

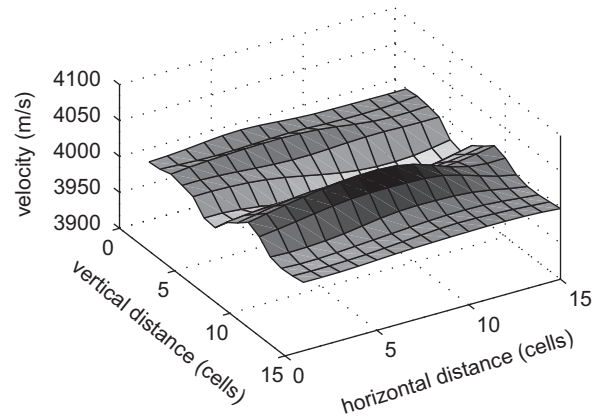


Fig. 16. Example 4—simple reef model. VSP geometry data acquisition. Reconstruction with best regularization parameter obtained from Fig. 15.

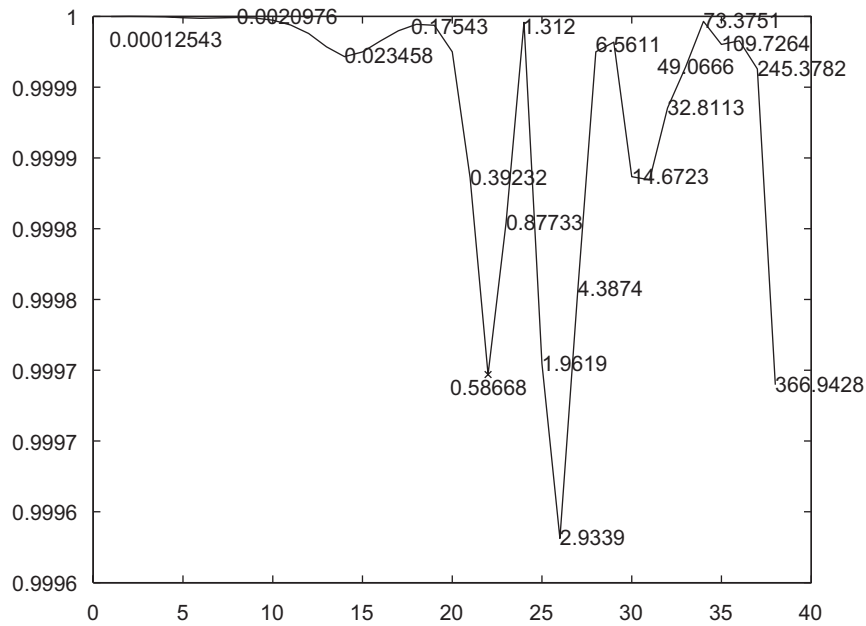


Fig. 17. Example 4—simple reef model. VSP geometry data acquisition. Θ -curve for second order.

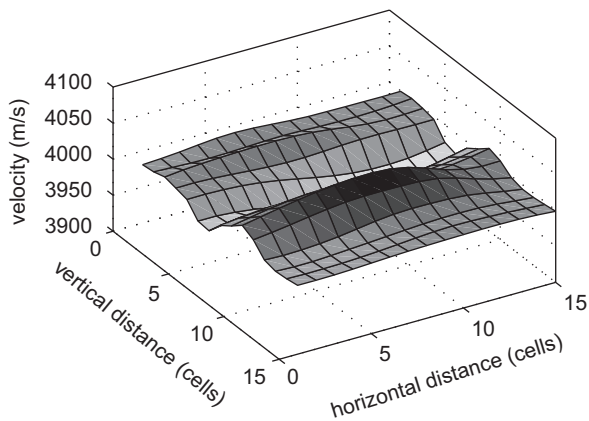


Fig. 18. Example 4—simple reef model. VSP geometry data acquisition. Reconstruction with best regularization parameter obtained from Fig. 17.

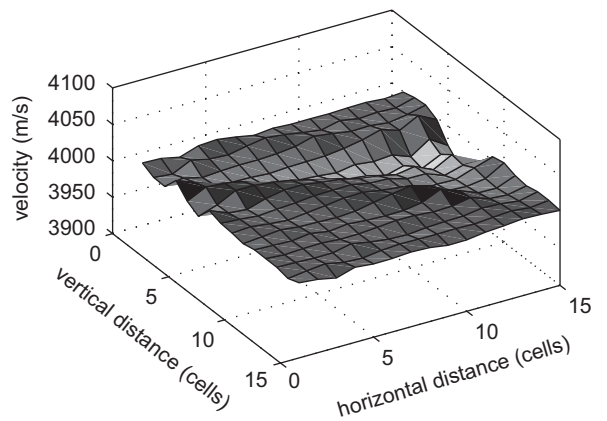


Fig. 19. Example 4—simple reef model. VSP geometry data acquisition. Least-squares reconstruction.

Fig. 15 shows the L-curve for second order and Fig. 16 shows the reconstruction. Here the L-curve obtained is more or less like the letter L shape, although the corner location is not obvious. For the same order, the Θ -curve can be seen in Fig. 17 and the reconstructed tomogram in Fig. 18. The results obtained using both criteria for the selection of the optimum regularization parameter were very similar in this case. We may also observe similar ϵ_{rms}^c estimators for both criteria. The least-squares solution is presented in Fig. 19. Once more the

result without regularization shows clearly the necessity of regularization combined with appropriate selection of the optimum regularization parameter.

5. Conclusions

From four sets of overdetermined synthetic examples corrupted by noise and with an ill-conditioned kernel matrix we have shown that the regularization algorithm in question, together with

its related approaches for the selection of the regularization parameter, is feasible in linear geophysical diffraction tomography. The two last sets represent the same simple geological model but with different acquisition geometries, cross-hole and VSP, this last one very common in geophysical exploration for hydrocarbon reservoirs. The comparison with non-regularized solution confirms the necessity of some kind of regularization. We considered three orders of regularization, where the order of regularization is equivalent to the order of the derivative matrix. One crucial aspect here is the selection of regularization parameter, usually chosen by some trial and error approach. We used the L-curve and we proposed a variation of it, which we named Θ -curve. The results were consistent, providing good to excellent approximations of the true model, even considering that Gaussian noise was always added to the scattered field, and the observed data was not exact, i.e., it did not come from the first-order Born series, but from a finite differences scheme. Natural extensions of this work are the application of this formulation to a layered medium background, and application to real data waveform.

Acknowledgments

This work is part of the projects “Multi-dimensional and spectral seismic processing in high-resolution seismo-stratigraphy” (edict CTPETRO/CNPq-FINEP 03/2001), and “Development of techniques and algorithms for improvement of subsurface imaging and seismic processing” (edict CTPETRO/CNPq 01/2003). The authors also would like to thank the support from PETROBRAS.

References

- Bassrei, A., Rodi, W.L., 1993. Regularization and inversion of linear geophysical data. In: Proceedings of the Third International Congress of the Brazilian Geophysical Society, Rio de Janeiro, Brazil, vol. 1, pp. 111–116.
- Belge, M., Kilmer, M.E., Miller, E.L., 2002. Efficient determination of multiple regularization parameters in a generalized L-curve framework. *Inverse Problems* 18, 1161–1183.
- Bouman, C., Sauer, K., 1993. A generalized gaussian image model for edge-preserving map estimation. *Institute of Electrical and Electronics Engineers Transactions on Image Processing* 2, 296–310.
- Calvetti, D., Golub, G.H., Reichel, L., 1999. Estimation of the L-curve via Lanczos bidiagonalization. *BIT (Nordisk Tidsskrift for Informationsbehandling)* 39, 603–619.
- Calvetti, D.P., Hansen, P.C., Reichel, L., 2002. L-curve curvature bounds via Lanczos bidiagonalization. *Electronic Transactions on Numerical Analysis* 14, 20–35.
- Castellanos, J.L., Gomez, S., Guerra, V., 2002. The triangle method for finding the corner of the L-curve. *Applied Numerical Mathematics* 43, 359–373.
- Devaney, A.J., 1984. Geophysical diffraction tomography. *Institute of Electrical and Electronics Engineers Transactions on Geoscience and Remote Sensing* 22, 3–13.
- Farquharson, C.G., Oldenburg, D.W., 2004. A comparison of automatic techniques for estimating the regularization parameter in non-linear inverse problems. *Geophysical Journal International* (156), 411–425.
- Hanke, M., 1996. Limitation of the L-curve method in ill-posed problems. *BIT (Nordisk Tidsskrift for Informationsbehandling)* 36, 287–301.
- Hanke, M., Raus, T., 1996. A general heuristic for choosing the regularization parameter in ill-posed problems. *Society for Industrial and Applied Mathematics Journal on Scientific Computing* 17, 956–972.
- Hansen, P.C., 1992. Analysis of discrete ill-posed problems by means of the L-curve. *Society for Industrial and Applied Mathematics Review* 34, 561–580.
- Hansen, P.C., 1998. Rank-deficient and Discrete Ill-posed Problems—Numerical Aspects of Linear Inversion. *Society for Industrial and Applied Mathematics, Philadelphia*, 247pp.
- Hansen, P.C., O’Leary, D.P., 1993. The use of the L-curve in the regularization of discrete ill-posed problems. *Society for Industrial and Applied Mathematics Journal on Scientific Computing* 14, 1487–1503.
- Kilmer, M.E., O’Leary, D.P., 2001. Choosing Regularization Parameters in Iterative methods for ill-posed problems. *Society for Industrial and Applied Mathematics Journal on Matrix Analysis and Applications* 22, 1204–1221.
- Lo, T.-W., Inderwiesien, P.L., 1994. Fundamentals of Seismic Tomography. *Geophysical Monograph Series*, Tulsa, OK, 178pp.
- McCarthy, P.J., 2003. Direct analytic model of the L-curve for Tikhonov regularization parameter selection. *Inverse Problems* 19, 643–663.
- Ray, R.D., Sanchez, B.V., 1994. Improved smoothing of a altimetric ocean-tide model with global Proudman functions. *Geophysical Journal International* 118, 788–794.
- Reginska, T., 1996. A regularization parameter in discrete ill-posed problems. *Society for Industrial and Applied Mathematics Journal on Scientific Computation* 17, 740–749.
- Reiter, T.D., Rodi, W.L., 1996. Nonlinear waveform tomography applied to crosshole seismic data. *Geophysics* 61, 902–913.
- Rocha Filho, A.A., Harris, J.M., Bassrei, A., 1996. A simple matrix formulation diffraction tomography algorithm. In: Proceedings of the 39th Brazilian Congress of Geology, Salvador, Brazil, vol. 2, pp. 312–315.
- Rocha Filho, A.A., Harris, J.M., Bassrei, A., 1997. Integrated inversion of seismic data using diffraction tomography. In: Proceedings of the Fifth International Congress of the Brazilian Geophysical Society, São Paulo, Brazil, vol. 2, pp. 630–634.

- Slaney, M., Kak, A.C., Larsen, L.E., 1984. Limitation of imaging with first-order diffraction tomography. *Institute of Electrical and Electronics Engineers Transactions on Microwave Theory and Techniques* 32, 860–874.
- Soupios, P.M., Papazachos, C.B., Juhlin, C., Tsokas, G.N., 2001. Nonlinear three-dimensional travelttime inversion of crosshole data with an application in the area of Middle Urals. *Geophysics* 66, 627–636.
- Soupios, P.M., Papazachos, C.B., Vallianatos, F., Papakostas, T., 2003. Numerical treatment and inspection of inverse problems. *World Scientific and Engineering Academy and Society Transactions on Circuits and Systems* 2, 547–552.
- Thompson, D.R., Rodi, W.L., Toksöz, M.N., 1994. Nonlinear seismic diffraction tomography using minimum structure constraints. *Journal of the Acoustical Society of America* 95, 324–330.
- Titterton, D.M., 1985. General structure of regularization procedures in image reconstruction. *Astronomy and Astrophysics* 144, 381–387.
- Twomey, S., 1963. On the numerical solution of Fredholm integral equations of the first kind by the inversion of the linear system produced by quadrature. *Journal of the Association of Computing Machines* 10, 97–101.
- Vogel, C.R., 1996. Non-convergence of the L-curve regularization parameter selection method. *Inverse Problems* 12, 535–547.
- Wu, R.-S., Toksöz, M.N., 1987. Diffraction tomography and multisource holography applied to seismic imaging. *Geophysics* 52, 11–25.
- Yao, Z.S., Roberts, R.G., 1999. A practical regularization for seismic tomography. *Geophysical Journal International* 138, 293–299.